PERGAMON

International Journal of Solids and Structures 40 (2003) 3273–3291

INTERNATIONAL JOURNAL OF SOLIDS and STRUCTURES

www.elsevier.com/locate/ijsolstr

Boundary element analysis of crack problems in functionally graded materials

Z.Q. Yue [a,*], H.T. Xiao [b], L.G. Tham [a]

[a] *Department of Civil Engineering, The University of Hong Kong, Pokfulam Road, Hong Kong*
[b] *Department of Engineering Mechanics, Shandong University of Science and Technology, Taian, China*

Received 26 August 2002; received in revised form 14 January 2003

Abstract

The present study examines the crack problems in a functionally graded material (FGM) whose upper and bottom surfaces are fully bonded with dissimilar homogeneous materials. A so-called generalized Kelvin solution based boundary element method is used in the numerical examination. The multi-region method and the eight-node traction-singular boundary elements are used for the crack evaluation. The layer discretization technique is utilized to approximate the depth material non-homogeneity of the FGM layer. The proposed method can deal with any depth variations in both the shear modulus and the Poisson ratio of the FGMs. Results of the present analysis are compared very well with the exact analytical solutions available in the literature, which demonstrates that the proposed method can accurately evaluate the stress intensity factors (SIFs) for cracks in FGMs. The paper further evaluates the effect of the functionally graded variations in the Poisson ratio on the stress intensity factors. The paper also assesses the elliptical cracks in the FGM system. The paper presents the influence of both the non-homogeneity and the thickness of the FGM layer on the three SIFs associated with the elliptical cracks.

Keywords: Boundary element method; Generalized Kelvin solution; Functionally graded materials; Stress intensity factors; Penny-shaped crack; Elliptical crack

1. Introduction

Functionally graded materials (FGMs) are applicable to many engineering fields. For example, some advanced turbine systems and earth-to-orbit winged planes use FGMs to achieve high efficiency and high velocity and to protect some components from high temperature. FGMs for use at high temperature are special composites that are usually made of ceramics and metals. In FGMs, the composite medium is processed in such a way that the material properties are continuous functions of the depth or thickness coordinate. The ceramics in an FGM offers thermal barrier effects and protects the metal from the metal

* Corresponding author. Tel.: +852-2859-1967; fax: +852-2559-5337.
E-mail address: yueqzq@hkucc.hku.hk (Z.Q. Yue).

0020-7683/03/$ - see front matter © 2003 Elsevier Science Ltd. All rights reserved.
doi:10.1016/S0020-7683(03)00094-5

corrosion and oxidation whilst the metallic composition toughs and strengthens the FGM (Jin and Batra, 1996; Chen and Erdogan, 1996).

The knowledge of fracture mechanics in FGMs is important in order to evaluate their integrity. Crack problems in FGMs have become one of the hottest topics of active investigation in fracture mechanics (Erdogan, 2000). By assuming an exponential variation of the elastic modulus in depth, Atkinson and List (1978), Dhaliwal and Singh (1978) and Delale and Erdogan (1983) examined the crack problems in non-homogeneous solids subjected to mechanical loads. Delale and Erdogan (1988) further examined the interface crack problems in bonded materials with a FGM under a plane strain condition. Erdogan and Ozturk (1992) found the solution of interface crack problems in bonded materials with a FGM subject to antiplane shear loading. Erdogan et al. (1991a,b) investigated the plane elasticity problem for two bonded half-planes containing a crack perpendicular to the interface and the mode III crack problem for two bonded homogeneous half planes, respectively. Ozturk and Erdogan (1996, 1995) further investigated the crack problems in the medium of two homogeneous half spaces bonded through a FGM layer containing a penny-shaped interface crack and subjected to either torsion or tension.

In the above investigations, both the analytical methods such as integral equations (see Ozturk and Erdogan, 1996) and the finite element method (e.g., Kim and Paulino, 2002; Gu et al., 1999) have been employed to solve the crack problems in FGMs. It is well known that the boundary element method (BEM) is one of the techniques that are particularly applicable to the calculation of stress singularities at crack front where high accurate results are expected. As a result, BEM has been widely used in the analysis of fracture mechanics (for review and references see Aliabadi, 1997). Another important feature associated with BEM is that it only requires the discretization of the boundary elements. An examination of the relevant literature available to the authors, however, indicates that there are few studies on crack problems in FGMs using the powerful BEM (e.g., Yuuki and Cho, 1989; Pan and Amadei, 1999).

In the present study, we are going to use a novel BEM for the evaluation of fracture intensity factors for cracks in FGMs. The novel BEM is the generalized Kelvin solution based boundary element method (GKS-BEM) (Yue and Xiao, 2002). The GKS-BEM is based on the GKS in multi-layered elastic solids (Yue, 1995). The GKS is the solution of a multi-layered elastic solid of infinite extent subject to the actions of concentrated point body forces. An important feature of Yue's solution is that the stresses, strains and displacements in the multi-layered elastic solids with arbitrary number of dissimilar layers can be calculated with controlled accuracy and high efficiency. Yue and Xiao (2002) have incorporated Yue's solution in the BEM formulation. The numerical results have shown that the BEM can be used to solve crack problems in multi-layered solids. In particular, the GKS-BEM is powerful in examining the crack problems in a layered solid comprising a large number of dissimilar layers. In this study, we will extend the GKS-BEM to the analysis of crack problems in FGMs.

In the GKS-BEM, the modified multi-region method is used in treating the two co-planar crack surfaces. The eight-node traction-singular elements are introduced in representing the displacements and tractions in the vicinity of a crack tip. The layered discretization technique is employed to represent the FGMs as a system of many piece-wisely homogeneous layers. In particular, we examine the crack problems for two dissimilar homogeneous materials fully bonded through a solid layer comprising a FGM. Fig. 1 illustrates the coordinate system for the crack problems where either a penny-shaped crack or an elliptical crack is located on the $z = 0$ plane. This model is a simplified version of a class of physical problems where cracks happen in ceramic coatings, metal/ceramic composites and interfacial zones with continuously varying volume fractions or graded properties (Ozturk and Erdogan, 1996).

At first, we will briefly present the GKS-BEM. In particular, we introduce a technique to handle the presence of infinite domains. Next, we will present a numerical evaluation of the crack problem that was examined analytically by Ozturk and Erdogan (1996). For this example, the FGM shear modulus is assumed to be $\mu_2 = \mu_1 \exp(\alpha z)$. The shear modulus of the bottom layer is assumed to be μ_1 whilst the shear modulus of the upper layer is $\mu_3 = \mu_1 \exp(\alpha h)$, where h is the thickness of the FGM layer. A comparison

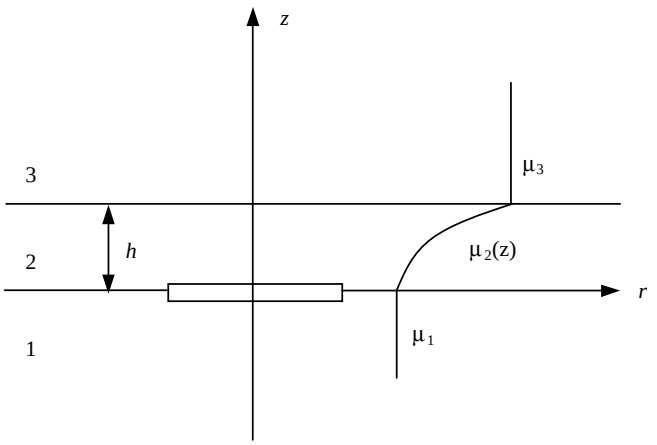

Fig. 1. Geometry and coordinates for the crack problem in a two dissimilar homogeneous material bonded through a non-homogeneous interfacial zone.

between the present results and the results given by Ozturk and Erdogan (1996) demonstrates that the proposed GKS-BEM can accurately calculate the stress intensity factors (SIFs) for the interface crack in bonded materials with a FGM.

We further examine the crack problem by assuming that both the elastic modulus and the Poisson ratio of the FGM layer are exponential functions of the vertical coordinate z. The paper evaluates the influence of the Poisson ratios of the homogeneous materials and the FGM on the SIFs of the penny-shaped crack. We then apply the GKS-BEM to examine the SIFs for an elliptical crack in the FGM system and examine the influence of the FGM non-homogeneity and thickness on the three SIFs associated with an elliptical crack.

2. The generalized Kelvin solution based boundary element method

In the ensuing, we will present a brief description of the GKS-BEM. More details of the mathematical formulation for this GKS-BEM can be found in Yue and Xiao (2002).

2.1. The generalized Kelvin solution

For an ease of reference, the GKS presented by Yue (1995) is outlined briefly in the ensuing. The GKS is the analytical solution for the elastostatic field in a layered solid of infinite extent due to the action of concentrated point loads. The total number of the dissimilar layers is an arbitrary integer n. The dissimilar homogeneous layers adhere an elastic solid of upper semi-infinite extent and another elastic solid of lower semi-infinite extent. The interface between any two connected dissimilar layers is fully bonded. By referring to Fig. 2, the jth layer occupies a finite layer region $H_{j-1} \leqslant z \leqslant H_j$ of thickness h_j ($h_j = H_j - H_{j-1}$), and has the shear modulus μ_j and the Poisson ratio v_j, where $j = 1, 2, 3, \ldots, n$. The 0th layer occupies the upper semi-infinite region $-\infty < z \leqslant 0$, and has the shear modulus μ_0 and the Poisson ratio v_0. The $(n+1)$ th layer occupies the lower semi-infinite region $H_n \leqslant z < \infty$ and has the shear modulus μ_{n+1} and the Poisson ratio v_{n+1}. Without loss of generality, it is assumed that the point load (F_x, F_y, F_z) is concentrated at a point $(0, 0, d)$ in the k th layer $(H_{k-1} \leqslant d \leqslant H_k)$. Details of the GKS can be found in Yue (1995), Yue et al. (1999)

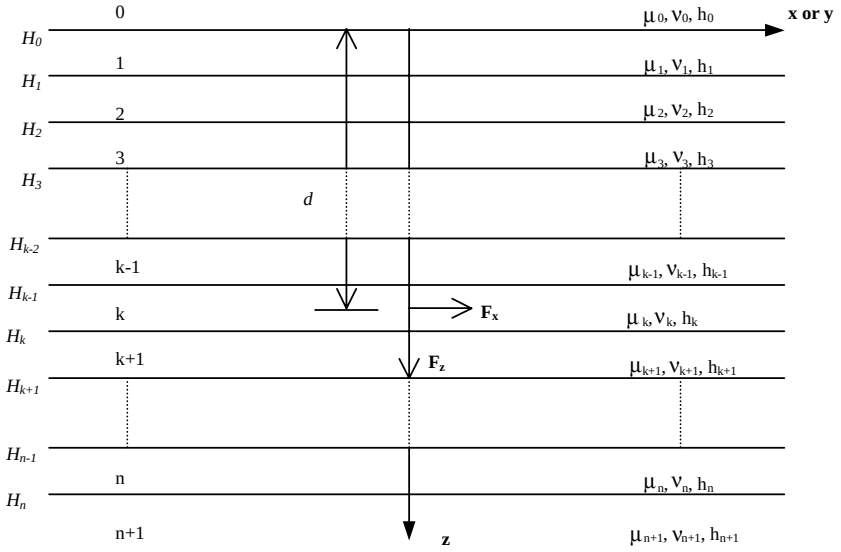

Fig. 2. A multi-layered elastic solid of infinite extent subjected to the body forces F_x and F_z concentrated at a point $(0, 0, d)$.

and Yue and Xiao (2002). In this study, the FGM layer is discretized as a system of n number of fully bonded dissimilar sub-layers.

2.2. The boundary integral equations

The numerical formulation of the GKS-BEM in multi-layered elastic solids using the GKS can be briefly summarized in the following. When the body forces are absent, the boundary integral equations for Yue's fundamental solutions can be expressed as follows:

$$C_{ij}(\boldsymbol{P})u_j(\boldsymbol{P}) = \int_S u^*_{ij}(\boldsymbol{P},\boldsymbol{Q})t_j(\boldsymbol{Q})\,\mathrm{d}S(\boldsymbol{Q}) - \int_S t^*_{ij}(\boldsymbol{P},\boldsymbol{Q})u_j(\boldsymbol{Q})\,\mathrm{d}S(\boldsymbol{Q}) \tag{1a}$$

where u_j and t_j are, respectively, the displacements and tractions on the boundary surface S; u^*_{ij} and t^*_{ij} are the displacements and tractions of the GKS; $\boldsymbol{P}$ and $\boldsymbol{Q}$ denote, respectively, the source and integration points on S; and C_{ij} is a coefficient dependent on the local boundary geometry at the source point $\boldsymbol{P}$. The C_{ij} can be evaluated using the following equations,

$$C_{ij}(\boldsymbol{P}) = \lim_{\varepsilon\to 0}\int_{S_\varepsilon} t^*_{ij}(\boldsymbol{P},\boldsymbol{Q})\,\mathrm{d}S(\boldsymbol{Q}) \tag{1b}$$

where S_ε is an infinitesimal spherical surface of center $\boldsymbol{P}$ and radius ε enclosed in the solids.

It is noted that Eq. (1a) does not contain the integration on the layer interface surfaces because the GKS strictly satisfies the interface conditions. So, it is not necessary to have the discretization along the layer interfaces in this BEM formulation. Eq. (1a) can be discretized to obtain a set of linear equation system for the solution of unknown boundary displacements and tractions.

2.3. Numerical methods for crack tips in FGMs

It has been shown that the crack-tip field singularities and angular distributions in FGMs are as the same as those in homogeneous elastic solids provided that the properties of the material are continuous and piecewise differentiable (see Delale and Erdogan, 1983; Jin and Noda, 1994). The result is independent of the form for material properties and the orientation of the crack. A detailed discussion on this subject can be found in Gu and Asaro (1997).

The influence of the material gradients at the near crack tip manifests itself through the SIF. For the crack problems under consideration, the stress state near the crack tip would always have the standard square-root singularity provided $h > 0$ (Ozturk and Erdogan, 1996). Therefore, we can use the ordinary BEM modeling developed for the regular square-root singularity for the present crack problem in the FGM system. The computational methods for the SIF in homogeneous solids can further be adopted to calculate the SIF for the penny-shaped crack and the elliptical crack in the FGM system. In the following, the numerical methods adopted in GKS-BEM for the crack problems in FGMs are briefly introduced.

The eight-node isoparametric element is usually employed to discretize the boundary surfaces. The numerical evaluations associated with the eight-node isoparametric elements have been very well discussed in Lachat and Waston (1976). The isoparametric element, however, may not be able to effectively and accurately model the displacement and stress fields near the crack tip. This is because the leading terms of the asymptotic expansions for the displacements and stresses near a crack tip in a homogeneous solid have the order of $r^{1/2}$ and $r^{-1/2}$, respectively, where r is the distance from the crack tip to a point within the solid. It is evident that the ordinary polynomials are not able to model these behaviors. Special boundary elements exactly containing the leading terms are usually used to represent the displacement and stress fields near the crack tip. Several singular elements are available for modeling the behavior near the crack tip (Aliabadi, 1997). In this study, we adopted the traction-singular elements to model the singular fields around the crack tip. Fig. 3 illustrates the shape functions of the traction-singular elements. They can be expressed as follows (Luchi and Rizzuti, 1987; Jia et al., 1989).

For displacements, we have:

$$N_d^i = \tfrac{1}{4}(1+\xi\xi_i)[1-\eta_i+\sqrt{2}\sqrt{1+\eta}\eta_i][\xi\xi_i+\sqrt{1+\eta}(\sqrt{1+\eta_i}+\eta_i)-\xi_i\sqrt{1+\eta_i}-\xi_i(1+\eta_i)] \quad \text{for } i=1,2,3,4 \tag{2a}$$

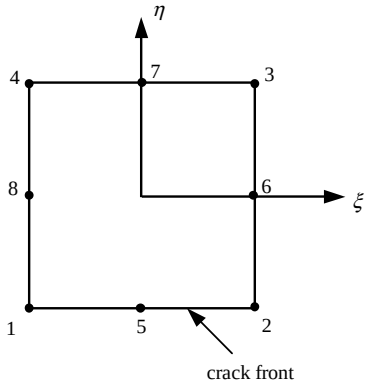

Fig. 3. A traction-singular element.

$$N_{\mathrm{d}}^{i}=\tfrac{1}{2}\xi_i^2(1+\xi\xi_i)[(\sqrt{2}+2)\sqrt{1+\eta}-(1+\sqrt{2})(1+\eta)]+\tfrac{1}{2}\eta_i^2[1-\eta_i+\sqrt{2}\sqrt{1+\eta}\eta_i](1-\xi^2)$$
$$\text{for } i=5,6,7,8 \tag{2b}$$

For tractions, we have:

$$N_{\mathrm{t}}^{i}=\frac{1}{\sqrt{1+\eta}}N_{\mathrm{d}}^{i}\quad \text{for } i=1,2,5 \tag{3a}$$

$$N_{\mathrm{t}}^{i}=\frac{\sqrt{1+\eta_i}}{\sqrt{1+\eta}}N_{\mathrm{d}}^{i}\quad \text{for } i=3,4,6,7,8 \tag{3b}$$

The shape functions (2) are used for the elements adjacent to a crack front on the crack faces or on the auxiliary boundary surfaces. The shape functions (3) are used only for the elements closely adjacent to the crack front on the auxiliary boundary surfaces, where the traction is singular.

For the discretization formulation of Eq. (1a) and when element l belongs to the traction-singular one, we have the following integrals in the intrinsic coordinates (ξ,η):

$$\boldsymbol{A}_{kj}=\int_{S_l}N_{\mathrm{t}}^{i}(\boldsymbol{Q}(\xi,\eta))u_{kj}^{*}(\boldsymbol{Q}(\xi,\eta),\boldsymbol{P})\boldsymbol{J}(\xi,\eta)\,\mathrm{d}\xi\,\mathrm{d}\eta \tag{4}$$

$$\boldsymbol{B}_{kj}=\int_{S_l}N_{\mathrm{d}}^{i}(\boldsymbol{Q}(\xi,\eta))t_{kj}^{*}(\boldsymbol{Q}(\xi,\eta),\boldsymbol{P})\boldsymbol{J}(\xi,\eta)\,\mathrm{d}\xi\,\mathrm{d}\eta \tag{5}$$

where u_{kj}^{*} has the singularity of the order r^{-1} and t_{kj}^{*} has the singularity of the order r^{-2} as $r\to 0$, where r is the distance from the source point $\boldsymbol{P}$ to the boundary field point $\boldsymbol{Q}$.

Higher order singularities in the integrands can occur because of the introduction of the special shape functions in the traction-singular elements. As a result, the numerical quadrature proposed by Luchi and Rizzuti (1987) was used to solve the singular integrals. A sequence of coordinate transformations with subdivision of the singular elements was used to remove the singularities from the integrands. Nine different cases are to be dealt with in evaluating the above integrals, depending on the location of the source point $\boldsymbol{P}$ (taken at nodal points only). More detailed discussions on the relevant topics may be found in Luchi and Rizzuti (1987).

It is noted that a great number of the kernel functions for the eight-node isoparametric and traction-singular elements in Eqs. (4) and (5) have to be evaluated. Because the GKS was expressed in a simple unified matrix form, we used limited computational time to calculate the kernel functions for a FGM system with a large number of the different layers.

2.4. Stress intensity factors calculations

After having obtained the numerical solution of the stresses and displacements in the FGM system containing the penny-shaped or elliptical cracks, we can determine the SIF values using the present GKS-BEM. The SIF values are related to the asymptotic behavior of stresses and displacements near the crack tip. Using the traction-singular elements, we can obtain the SIF values by displacement extrapolation from two nodal values. The extrapolation procedure involves the correlation of the computed displacements and tractions with the theoretical values and extrapolates them to the crack front (Luchi and Rizzuti, 1987). To show this procedure, we consider the crack front with the elements in Fig. 4.

For a mixed mode problem in which modes I, II and III are present, their corresponding SIF values K_{I}, K_{II} and K_{III} at the corner point C in Fig. 4 can be linearly extrapolated from the computed crack face opening displacements at the nodes $A-A'$ and $B-B'$ as follows:

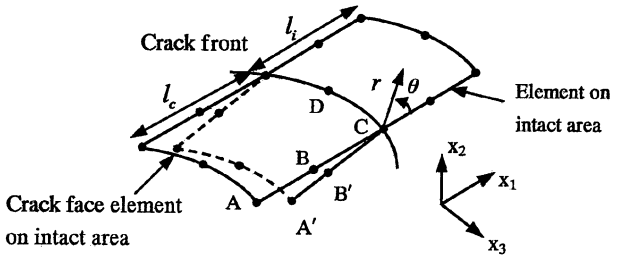

Fig. 4. Crack front elements.

$$K_{\mathrm{I}} = \frac{E}{4(1-\nu^2)}\sqrt{\frac{\pi}{2}}\frac{2\sqrt{2}(u_2^B - u_2^{B'}) - (u_2^A - u_2^{A'})}{\sqrt{l_c}} \tag{6a}$$

$$K_{\mathrm{II}} = \frac{E}{4(1-\nu^2)}\sqrt{\frac{\pi}{2}}\frac{2\sqrt{2}(u_1^B - u_1^{B'}) - (u_1^A - u_1^{A'})}{\sqrt{l_c}} \tag{6b}$$

$$K_{\mathrm{III}} = \frac{E}{4(1+\nu)}\sqrt{\frac{\pi}{2}}\frac{2\sqrt{2}(u_3^B - u_3^{B'}) - (u_3^A - u_3^{A'})}{\sqrt{l_c}} \tag{6c}$$

This linear extrapolation procedure decouples the fracture modes I and II when the intact plane coincides with the crack plane. In this case, the angle θ is zero. In Eqs. (6a)–(6c), l_c denotes the length of the crack element adjacent to the crack front, and is measured perpendicular to the crack front.

2.5. Treatment of cracks in infinite domain

The FGM system in Fig. 1 occupies a region of infinite domain. In solving the crack problems in infinite domains, a popular strategy used in BEM is to approximate the infinite body by a large finite body. This treatment usually suffers two drawbacks, namely, large numbers of degrees of freedom and/or poor accuracy. To overcome these drawbacks, Jia et al. (1989) presented a modified multi-region method for solving crack problems in three-dimensional infinite bodies. This method can be characterized by an exact representation of the infinite domain. Herein, the method is used to solve crack problems in the FGM system occupying an infinite domain.

We consider a multi-layered solid of infinite extent containing a crack of arbitrary shape in Fig. 5. The crack has two open surfaces. We can form the first closed curved surface by adding an open imaginary surface in the solid to one of the two crack surfaces. We can also form the second closed curved surface by adding the open imaginary surface in the solid to the other crack surface. The two closed curved surfaces divide the entire solid into two regions. We denote the region within the first closed curved surface as the region I. Its complement, the region outside the second closed curved surface is then denoted as the region II. Each of the two regions I and II has a crack face on its boundary. The open imaginary surface serves a common boundary for the two regions. The two crack faces are the actual boundaries. It is also noted that the two crack faces occupy the same area and are separated. There is no open space between the two crack faces before the load application.

Since the two regions share the same boundary geometry, the BIE's for both the regions are the same except for some signs change and slight differences in the $C_{ij}(\boldsymbol{p})$ terms. Therefore, the coefficient matrix for either I or II is sufficient to construct the matrix for the entire problem.

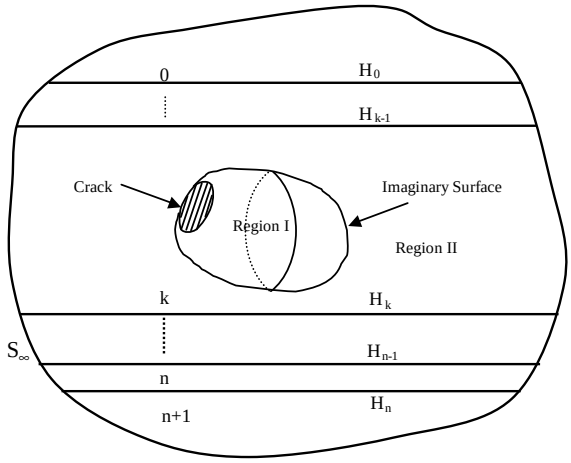

Fig. 5. Sketch illustrating the subdivision strategy for a crack in a multi-layered elastic solid.

Using the discretized boundary integral equations, the matrix equation for the region I can be written as

$$[\mathbf{A}]\{\mathbf{u}_\mathrm{I}\} = [\mathbf{B}]\{\mathbf{t}_\mathrm{I}\} \tag{7}$$

where the matrix **A** is obtained from the integrals containing t^*_{ij}; the matrix **B** is obtained from the integrals containing u^*_{ij}; $\mathbf{u}_\mathrm{I}$ and $\mathbf{t}_\mathrm{I}$ are the boundary displacements and tractions, respectively, for the region I.

The matrix equation for the region II is constructed by taking advantage of (7). It can be expressed as follows:

$$[-\boldsymbol{A}^*]\{\boldsymbol{u}_\mathrm{II}\} = [\boldsymbol{B}]\{\boldsymbol{t}_\mathrm{II}\} \tag{8}$$

where $\mathbf{A}^*$ is identical to **A** except for the diagonal terms, in which the contribution of the boundary at infinity has to be taken into consideration; **B** is the same for both the regions. We further use the continuity conditions for displacements and tractions over the common boundary,

$$\begin{aligned} \mathbf{u}_\mathrm{I} &= \mathbf{u}_\mathrm{II} \\ \mathbf{t}_\mathrm{I} &= -\mathbf{t}_\mathrm{II} \end{aligned} \tag{9}$$

Eqs. (7) and (8) are coupled. The equations for the entire problem domain can be written as

$$[\mathbf{G}]\{\mathbf{x}\} = \{\mathbf{R}\} \tag{10}$$

where **G** is the overall matrix of coefficients, its row and column numbers are equal to two times of the row and column numbers of the single domain matrix, respectively; **x** is the vector of the unknowns and consists of the displacements and tractions over the entire boundary except for the applied crack-face tractions. **R** is the known vector containing the effect of known crack-face tractions.

3. Numerical verifications

In the ensuing, we will apply the GKS-BEM to the examination of the crack problems in the FGM system. In this section, we will study the penny-shaped crack problems in bonded materials with a graded interfacial region. This problem has been solved recently by Ozturk and Erdogan (1996) using an integral transform method. So, we will compare the numerical results with those given by Ozturk and Erdogan (1996). After this numerical evaluation and verification, we will apply the GKS-BEM to examine the influence of the functionally graded Poisson's ratio on the SIF. In this application, we extended the crack

problem examined by Ozturk and Erdogan (1996) by allowing the Poisson ratio to be the exponential function of the vertical coordinate z. Next, we further apply the GKS-BEM to examine elliptical crack problems in the bonded materials with a graded interfacial region.

Ozturk and Erdogan (1996) analyzed the problem of a penny-shaped crack in two bonded materials with a graded interfacial region. In this study, we re-examined this problem to demonstrate the effectiveness and accuracy of the proposed numerical method in dealing with crack problems in the FGM system. The axisymmetric crack problem for the FGM solid is described in Fig. 1. The FGM system consists of two homogeneous materials bonded through a non-homogeneous interfacial region of thickness h. The penny-shaped crack (the radius $a = 1$) is subjected to a uniform tensile load p_0 normal to the crack faces. In this study, it is assumed that the Poisson ratio of the FGM system is constant (i.e. $v_1 = v_2 = v_3 = v$). The shear modulus μ_2 is approximated by

$$\mu_2(z) = \mu_1 \mathrm{e}^{\alpha z}, \tag{11a}$$

$$\alpha = \frac{1}{h} \log(\mu_3/\mu_1) \tag{11b}$$

where h is the thickness of the interfacial layer; the constant α can be positive or negative.

For convenience, we chose the surface of a hemisphere in a homogeneous material (material 1) to form the two regions for the BEM analysis. Because of symmetry, it was necessary only to analyze a quarter of the hemisphere, such that only this quarter is discretized, with no elements on the plane of symmetry. Fig. 6 shows the surface discretization in 289 nodes and 88 boundary elements, in which there are 16 traction-singular elements employed along the crack front. For $0 \leqslant z \leqslant h$, the FGM is closely approximated by n bonded layers of elastic homogeneous media. Each layer has the thickness equal to h/n and shear modulus equal to $\mu_2(z)$ at the top depth of the layer, i.e. for the ith layer, $z = H_i$, where $H_i = ih/n$, $(i = 1, 2, \ldots, n)$. Two homogeneous materials bonded through the FGM are considered as semi-infinite domains for the layers H_0 and H_{n+1} respectively. For all the layers, the Poisson ratios are the same and equal to 0.3. Fig. 7 illustrates an approximation of the continuous depth variation of the shear modulus by a large number of piece-wisely homogeneous layers, where $n = 20$, $h = 0.5$ and $\alpha = 3.0$. It can be observed from Fig. 7 that a close approximation of the shear modulus variation can be obtained using a large number of n.

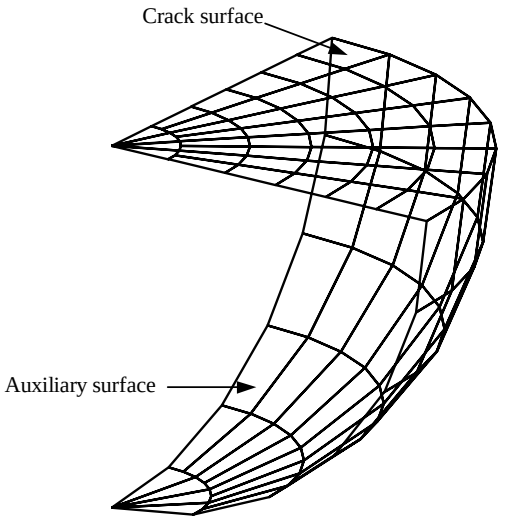

Fig. 6. Boundary element mesh of a penny-shaped crack.

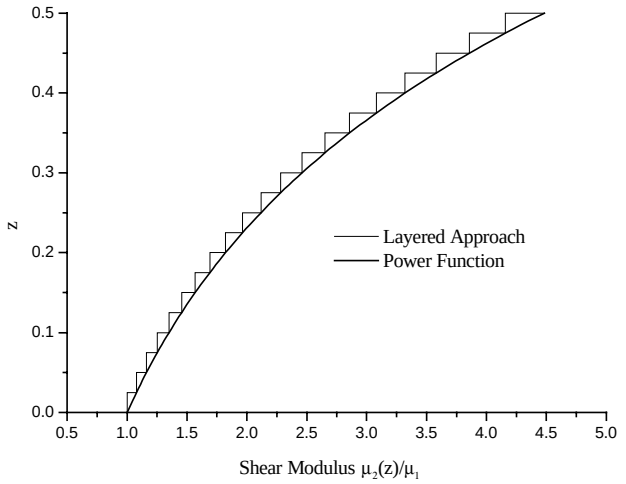

Fig. 7. Approximation of the continuous depth variation of the shear modulus by a layered system of 20 piece-wisely homogeneous layers at $\alpha = 3.0$ and $h = 0.5$.

We compared the GKS-BEM results with those given by Ozturk and Erdogan (1996). The following four cases: $\alpha = 0.4$, 0.6, 2.0 and 3.0 are analyzed using the layered approximations and the comparison results are shown in Table 1. From Table 1, it can be observed that the layered approximation ($n = 20$) resulted in excellent results for the SIF values. For $\alpha = 0.4$, the absolute differences between the results of the two methods are equal to 1.289% and 0.053% for the normalized SIF K_I and K_{II} values respectively. For $\alpha = 0.6$, the two absolute differences are equal to 1.3% and 0.12%. For $\alpha = 2.0$, the two absolute errors are equal to 0.85% and 0.59%. For $\alpha = 3.0$, the two absolute errors are equal to 0.03% and 0.21%.

Table 1
Results of the normalized SIF values by the present study and Ozturk and Erdogan (1996) at $h/a = 0.5$ and $v_1 = v_2 = v_3 = 0.3$

No. of a layered FGM	$\alpha = 0.4$		$\alpha = 0.6$		$\alpha = 2.0$		$\alpha = 3.0$	
	$\frac{K_I}{p_0\sqrt{\pi a}}$	$\frac{K_{II}}{p_0\sqrt{\pi a}}$	$\frac{K_I}{p_0\sqrt{\pi a}}$	$\frac{K_{II}}{p_0\sqrt{\pi a}}$	$\frac{K_I}{p_0\sqrt{\pi a}}$	$\frac{K_{II}}{p_0\sqrt{\pi a}}$	$\frac{K_I}{p_0\sqrt{\pi a}}$	$\frac{K_{II}}{p_0\sqrt{\pi a}}$
5	0.62253	0.01362	0.61030	0.02185	0.53497	0.06321	0.49312	0.07892
6	0.62340	0.01308	0.61153	0.02102	0.53918	0.06161	0.49810	0.07695
7	0.62395	0.01287	0.61197	0.02056	0.54126	0.06040	0.50265	0.07494
8	0.62462	0.01224	0.61343	0.01985	0.54524	0.05870	0.50740	0.07343
9	0.62487	0.01226	0.61378	0.01988	0.54593	0.05856	0.50799	0.07328
10	0.62547	0.01200	0.61389	0.01919	0.54745	0.05692	0.51013	0.07177
11	0.62549	0.01216	0.61469	0.01975	0.54735	0.05719	0.51021	0.07155
12	0.62584	0.01157	0.61529	0.01891	0.55085	0.05636	0.51509	0.07064
13	0.62536	0.01199	0.61455	0.01949	0.54940	0.05747	0.51317	0.07008
14	0.62617	0.01132	0.61570	0.01852	0.55184	0.05532	0.51592	0.06959
15	0.62651	0.01151	0.61621	0.01882	0.55156	0.05501	0.51480	0.06885
16	0.62618	0.01180	0.61567	0.01926	0.54991	0.05615	0.51425	0.07039
17	0.62668	0.01148	0.61645	0.01877	0.55318	0.05649	0.51760	0.07109
18	0.62671	0.01114	0.61654	0.01827	0.55471	0.05491	0.51739	0.06895
19	0.62601	0.01156	0.61554	0.01887	0.55292	0.05600	0.51836	0.07037
20	0.62619	0.01157	0.61577	0.01889	0.55210	0.05652	0.51747	0.07047
Ozturk and Erdogan	0.6133	0.0121	0.6026	0.0177	0.5436	0.0506	0.5135	0.0684

As the layer discretization number n increases, the SIF values (K_I and K_{II}) from the GKS-BEM stably approached to the exact solutions. The results presented in Table 1 demonstrated that accurate SIF values for crack problems in FGMs could be obtained by using the GKS-BEM together with the layered discretization technique. In the ensuing, we will present the results of applying the GKS-BEM to two crack problems in the FGM system. An examination of the relevant literature revealed that there were no publications available on the SIF values of the two cracks problems.

4. Further engineering applications

4.1. Application A: influence of Poisson's ratio

The crack problem in the FGM system examined by Ozturk and Erdogan (1996) adopted the assumption that the Poisson ratios of the three materials are constant and equal. They examined the effects of the Poisson ratios v on the normalized SIF values for fixed values of h/a and μ_3/μ_1. Their findings indicated that the Poisson ratios have limited effects on the SIF values in general whilst the effects are substantial for the relatively large negative values of αa or very small values of μ_3/μ_1 under the mode I loading.

In the ensuing, we will present the results of using the GKS-BEM to examine the effect of the Poisson ratios on the SIF values of the crack problem in the FGM system. We adopted the depth variation functions of the material modulus and Poisson ratio that were used by Gu and Asaro (1997) and Noda and Jin (1993) for cracks in FGM materials. The elastic modulus and Poisson's ratio of the FGM are assumed to vary with the depth z according to the following exponential rules:

$$E_2(z) = E_1 e^{\alpha_1 z}, \quad v_2(z) = v_1 e^{\alpha_2 z} \tag{12a}$$

where α_1 and α_2 are the material constants representing the material gradients; E_1 and v_1 are the values of elastic properties of the material 1. The parameters α_1 and α_2 have the dimension of 1/length. The elastic properties of the material 3 are described by

$$E_3 = E_1 e^{\alpha_1 h}, \quad v_3 = v_1 e^{\alpha_2 h} \tag{12b}$$

Fig. 1 shows the crack problem in the FGM system where the penny-shaped crack is located at $z = 0.0$ plane. The corresponding results are listed in Table 2. Similar to the results given by Ozturk and Erdogan (1996), the present results indicate that the SIF values do not change significantly with the changes of the Poisson ratio. The difference in the Poisson ratios between the material 1 and the FGM layer induces limited variations of the mode I and II SIF values. For the ratio E_3/E_1 is very small, the Poisson ratios have some evident effects on the mode I and II SIF values. In Table 2, it can be further observed that the mode II SIF values increase and the mode I SIF values decrease as α_1 increases.

4.2. Application B: elliptical crack problem

In the ensuing, we will present the GKS-BEM evaluation of an elliptical crack in the FGM system as shown in Fig. 1. The Poisson ratios of the materials 1 and 3 and the FGM layer are constant and equal to 0.3. The shear modulus μ_2 is governed by Eq. (11a). The crack parameter values, as shown in Fig. 8, are assumed to that $b/a = 0.5$ ($a = 1.0$) and $p_0 = 1$. The elliptical crack is located at the $z = 0$ plane in Fig. 1. For symmetry, we used only a quarter of the region for the GKS-BEM discretization. Fig. 9 shows the surface discretization results with 289 nodes and 88 boundary elements. In addition, we have 16 traction-singular elements used along the crack front. The two sides of traction-singular elements at the crack face are perpendicular to the tangent at the crack front of the elliptical crack. The two sides are intersected with the crack front. As a result, we can obtain the high accurate SIF values.

Table 2
Influence of the Poisson ratio on the SIF values of a penny-shaped crackat the condition $h/a = 0.5$, $v_1 = 0.01$ and $v_3 = v_1 e^{\alpha_2 h}$

v_3	$\alpha_1 = 1.0$		$\alpha_1 = 0.5$		$\alpha_1 = 0.1$	
	$\frac{K_I}{p_0\sqrt{\pi a}}$	$\frac{K_{II}}{p_0\sqrt{\pi a}}$	$\frac{K_I}{p_0\sqrt{\pi a}}$	$\frac{K_{II}}{p_0\sqrt{\pi a}}$	$\frac{K_I}{p_0\sqrt{\pi a}}$	$\frac{K_{II}}{p_0\sqrt{\pi a}}$
0.01	0.59108	0.05828	0.61847	0.02947	0.64126	0.00366
0.1	0.59210	0.05328	0.61967	0.02410	0.64259	−0.00210
0.2	0.59217	0.04884	0.61991	0.01933	0.64295	−0.00714
0.3	0.59079	0.04480	0.61916	0.01534	0.64175	−0.01141
0.4	0.58741	0.04101	0.61562	0.01166	0.63819	−0.01499
0.5	0.58099	0.03728	0.60864	0.00843	0.63089	−0.01778
	$\alpha_1 = -0.1$		$\alpha_1 = -0.5$		$\alpha_1 = -1.0$	
0.01	0.65243	−0.01029	0.67578	−0.03971	0.70150	−0.07608
0.1	0.65387	−0.01619	0.67749	−0.04590	0.70348	−0.08255
0.2	0.65437	−0.02137	0.67828	−0.05134	0.70469	−0.08824
0.3	0.65324	−0.02572	0.67738	−0.05578	0.70424	−0.09283
0.4	0.64969	−0.02923	0.67396	−0.05920	0.70127	−0.09613
0.5	0.64228	−0.03178	0.66646	−0.06129	0.69427	−0.09789

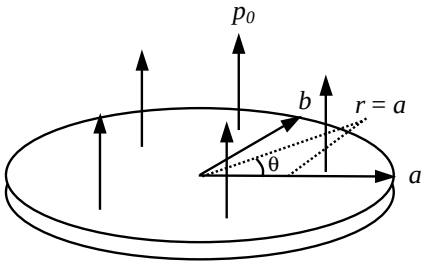

Fig. 8. An elliptical crack at the interface of a homogeneous and a FGM subject to a uniform tension load p_0.

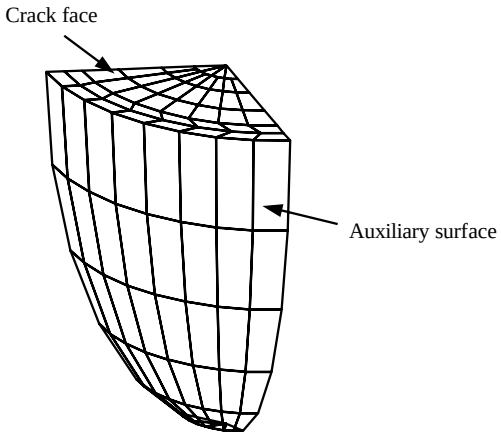

Fig. 9. Boundary element mesh for a quarter of an elliptical crack.

To verify the present method, we first examined the SIF values of an elliptical crack in a homogeneous solid using the GKS-BEM method. We found that the maximum absolute difference in the SIF values between the GKS-BEM method and the exact solution in Tada et al. (2000) was less than 1.00% along the crack tip. In order to further verify the GKS-BEM method for crack problems in FGM system, we adopted different numbers of layered approximations for the FGM layer. Table 3 shows that the SIF values (K_{I}, K_{II}, K_{III}) would become the steady values as the layer number n for the FGM layer increases. It is evident that the SIF trend to converge to a steady value as n becomes sufficiently large. Similar findings were also given in Wang et al. (2000) and Noda and Wang (2002).

Fig. 10 shows the results of the normalized crack opening displacement (COD) along the major axis of the elliptical axis in z-direction, $(w^+ - w^-)/w_0$. In Fig. 10, the normalization factor w_0 is the maximum relative crack surface displacement for the corresponding pressurized plane strain crack (the crack length, $2a$), i.e. $w_0 = (1+\kappa)p_0 a/2\mu_1$, $\kappa = 3 + 4v$. Note that for $\alpha = 0$, the COD corresponds to the case of a homogeneous medium.

Figs. 11 and 12 shows the influences of the material non-homogeneity parameter α on the SIF K_{I}, K_{II}, respectively. The corresponding SIF values are also listed in Tables 4 and 5. The influence of the material non-homogeneity parameter α on the mode III SIF K_{III} is given in Table 6. It can be observed in Fig. 11 that as α increases, the mode I SIF tends to decrease. This result is due to the increase in stiffness of the half

Table 3
The SIF values of an elliptical crack in the bonded materials through a FGM at $v_1 = v_2 = v_3 = 0.3$, $h/a = 0.5$ and $\alpha = 3.0$

No. of a layered FGM	$\theta = 0.000°$			44.999°			90.000°		
	$\frac{K_{\mathrm{I}}}{p_0}$	$\frac{K_{\mathrm{II}}}{p_0}$	$\frac{K_{\mathrm{III}}}{p_0}$	$\frac{K_{\mathrm{I}}}{p_0}$	$\frac{K_{\mathrm{II}}}{p_0}$	$\frac{K_{\mathrm{III}}}{p_0}$	$\frac{K_{\mathrm{I}}}{p_0}$	$\frac{K_{\mathrm{II}}}{p_0}$	$\frac{K_{\mathrm{III}}}{p_0}$
5	0.59199	0.07982	0.00000	0.72419	0.09278	0.01701	0.79517	0.10324	0.00000
10	0.61814	0.07039	0.00000	0.75519	0.07811	0.01720	0.82750	0.08538	0.00000
15	0.62670	0.06773	0.00000	0.76547	0.07395	0.01725	0.83827	0.08002	0.00000
20	0.62985	0.06627	0.00000	0.77068	0.07114	0.01712	0.84148	0.07765	0.00000
25	0.63338	0.06641	0.00000	0.77514	0.07103	0.01694	0.84873	0.07621	0.00000
30	0.63429	0.06507	0.00000	0.77581	0.06905	0.01708	0.84670	0.07521	0.00000
35	0.63640	0.06561	0.00000	0.77814	0.06935	0.01707	0.85175	0.07433	0.00000
40	0.63867	0.06490	0.00000	0.77933	0.07028	0.01733	0.85313	0.07494	0.00000
50	0.63913	0.06550	0.00000	0.78116	0.07052	0.01743	0.85538	0.07545	0.00000

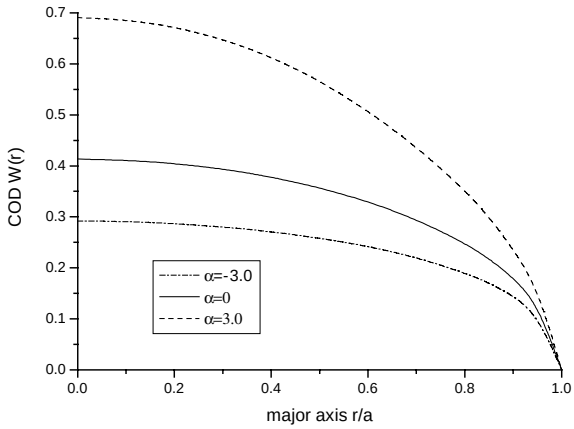

Fig. 10. Results for the z-component of the normalized COD along the major axis of an elliptical crack $w(r) = (w^+ - w^-)/w_0$ where $w_0 = (1+\kappa)p_0 a/2\mu_1$, $h/a = 0.5$ and $v = 0.3$.

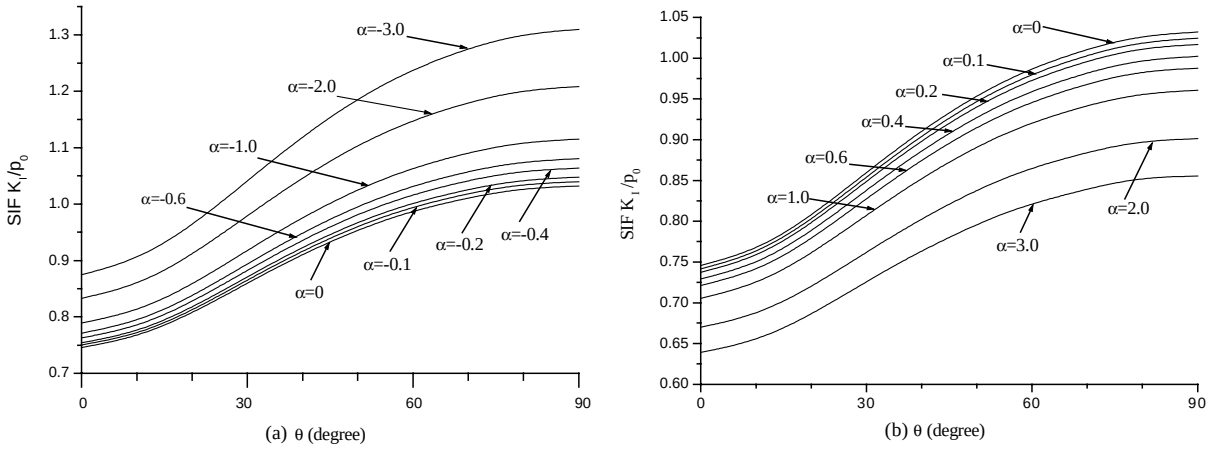

Fig. 11. Mode I SIF for an elliptical crack in the FGM with different α values at $h/a = 0.5$ and $v = 0.3$.

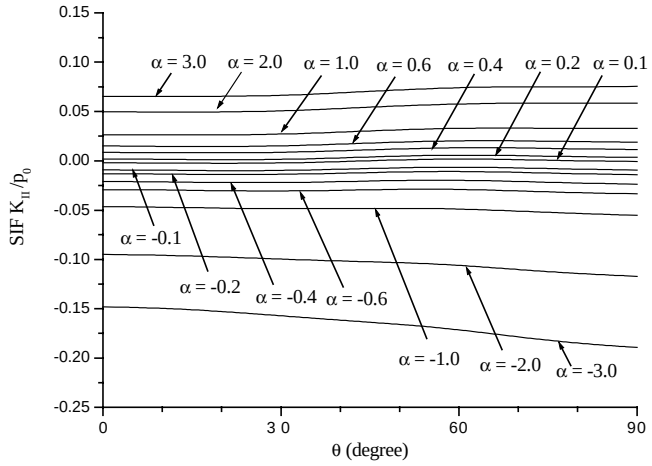

Fig. 12. Mode II SIF for an elliptical crack in the FGM with different α values at $h/a = 0.5$ and $v = 0.3$.

space $z > 0$. For a fixed α value, the mode I SIF value has a maximum value at the crack tip of the minor axis and a minimum value at the crack tip of the major axis. In Figs. 11 and 12, it can be shown that the mode II SIF values are considerably smaller than the mode I SIF values. As the absolute values of α decrease, the mode II SIF values tend to zero. In Table 6, the maximum absolute difference between the mode III SIF values estimated by the numerical method ($\alpha = 0$) and the exact solution in a homogeneous solid ($K_{III} = 0.0$) is 0.084%, which further indicates the GKS-BEM results are accurate. It is also clear that the mode III SIF values for the different α values are small by comparing the mode I and II SIF values in Tables 4 and 5.

We further carried out the analysis for many cases of h/a to examine the influence of the different values h/a on the SIF values. Figs. 13 and 14 show the variations of the mode I and II SIF values for an elliptical crack with h/a. The corresponding SIF values are also listed in Tables 7 and 8. Table 9 presents the variations of the mode III SIF with h/a. When $\mu_3 = \mu_1 \exp(\alpha h)$, $\alpha = 0.5$ and $h = 0.0$, the FGM system

Table 4
Variation of the SIF value (K_I/p_0) with α and θ at $h/a = 0.5$ and $a = 1.0$

θ (°)	α												
	−3.0	−2.0	−1.0	−0.6	−0.4	−0.2	0.0	0.2	0.4	0.6	1.0	2.0	3.0
0.000	0.87482	0.83276	0.78894	0.77134	0.76273	0.75426	0.74580	0.73745	0. 72928	0.72120	0.70548	0.66973	0.63913
11.248	0.90441	0.85897	0.81220	0.79370	0.78455	0.77558	0.76659	0.75773	0. 74910	0.74063	0.72433	0.68677	0.65495
22.499	0.97967	0.92574	0.87114	0.84971	0.83931	0.82894	0.81884	0.80893	0. 79903	0.78960	0.77115	0.72921	0.69502
33.749	1.07209	1.00622	0.94128	0.91615	0.90404	0.89223	0.88039	0.86903	0. 85773	0.84687	0.82579	0.77854	0.74148
44.999	1.15667	1.07858	1.00354	0.97495	0.96146	0.94778	0.93468	0.92190	0. 90912	0.89730	0.87377	0.82215	0.78116
56.250	1.22285	1.13535	1.05262	1.02157	1.00670	0.99207	0.97784	0.96400	0. 95052	0.93755	0.91274	0.85774	0.81496
67.500	1.26866	1.17389	1.08577	1.05281	1.03689	1.02137	1.00651	0.99205	0. 97783	0.96403	0.93774	0.88046	0.83542
78.750	1.30090	1.20123	1.10937	1.07492	1.05851	1.04274	1.02729	1.01229	0. 99792	0.98378	0.95676	0.89838	0.85369
90.000	1.30946	1.20829	1.11500	1.08048	1.06376	1.04770	1.03206	1.01688	1. 00222	0.98785	0.96075	0.90136	0.85538

Table 5
Variation of the SIF value (K_{II}/p_0) with α and θ at $h/a = 0.5$ and $a = 1.0$

θ (°)	α												
	−3.0	−2.0	−1.0	−0.6	−0.4	−0.2	0.0	0.2	0.4	0.6	1.0	2.0	3.0
0.000	−0.14817	−0.09481	−0.04646	−0.02925	−0.02104	−0. 01321	−0.00551	0.00181	0.00860	0.01497	0.02660	0.04962	0.06550
11.248	−0.14954	−0.09570	−0.04703	−0.02960	−0.02141	−0. 01349	−0.00586	0.00140	0.00825	0.01459	0.02633	0.04951	0.06532
22.499	−0.15360	−0.09802	−0.04817	−0.03057	−0.02233	−0. 01411	−0.00641	0.00090	0.00798	0.01436	0.02617	0.04938	0.06539
33.749	−0.15880	−0.10050	−0.04876	−0.03061	−0.02201	−0. 01363	−0.00576	0.00176	0.00891	0.01550	0.02746	0.05117	0.06679
44.999	−0.16380	−0.10241	−0.04835	−0.02923	−0.02043	−0. 01193	−0.00372	0.00405	0.01133	0.01803	0.03039	0.05457	0.07052
56.250	−0.16849	−0.10419	−0.04797	−0.02839	−0.01918	−0. 01050	−0.00208	0.00587	0.01322	0.02021	0.03275	0.05717	0.07350
67.500	−0.17688	−0.10919	−0.05045	−0.02993	−0.02033	−0. 01117	−0.00255	0.00560	0.01333	0.02057	0.03359	0.05855	0.07553
78.750	−0.18456	−0.11417	−0.05324	−0.03222	−0.02240	−0. 01306	−0.00414	0.00428	0.01215	0.01954	0.03286	0.05839	0.07478
90.000	−0.18923	−0.11724	−0.05517	−0.03358	−0.02356	−0. 01396	−0.00497	0.00352	0.01160	0.01910	0.03277	0.05853	0.07545

Table 6
Variation of the SIF value (K_{III}/p_0) with α and θ at $h/a = 0.5$ and $a = 1.0$

θ (°)	α												
	−3.0	−2.0	−1.0	−0.6	−0.4	−0.2	0.0	0.2	0.4	0.6	1.0	2.0	3.0
0.000	0.00000	0.00000	0.00000	0.00000	0.00000	0.00000	0.00000	0.00000	0.00000	0.00000	0.00000	0.00000	0.00000
11.248	−0.01881	−0.01227	−0.00602	−0.00373	−0.00263	−0.00163	0.00061	0.00035	0.00121	0.00204	0.00363	0.00647	0.00827
22.499	−0.03248	−0.02099	−0.01014	−0.00625	−0.00437	−0.00254	0.00084	0.00079	0.00236	0.00381	0.00635	0.01121	0.01412
33.749	−0.03916	−0.02505	−0.01183	−0.00713	−0.00484	−0.00264	0.00056	0.00143	0.00330	0.00502	0.00809	0.01391	0.01694
44.999	−0.03886	−0.02479	−0.01154	−0.00672	−0.00449	−0.00235	0.00024	0.00176	0.00356	0.00528	0.00841	0.01413	0.01743
56.250	−0.03267	−0.02078	−0.00955	−0.00545	−0.00355	−0.00172	−0.00005	0.00171	0.00329	0.00472	0.00729	0.01208	0.01460
67.500	−0.02364	−0.01499	−0.00683	−0.00386	−0.00244	−0.00109	−0.00020	0.00143	0.00254	0.00363	0.00553	0.00899	0.01193
78.750	−0.01220	−0.00768	−0.00341	−0.00183	−0.00111	−0.00042	−0.00025	0.00088	0.00147	0.00202	0.00308	0.00486	0.00568
90.000	0.00000	0.00000	0.00000	0.00000	0.00000	0.00000	0.00000	0.00000	0.00000	0.00000	0.00000	0.00000	0.00000

degenerates as a homogeneous solid. In this degenerated system, the corresponding SIF are presented in the handbook of the SIFs (Tada et al., 2000). In Figs. 13 and 14, we can observe that the mode I and II SIF values have different variation patterns as the h/a increases. As the h/a increases, the mode I SIF values decreases whilst the mode II SIF values increase. In general, the mode I and II SIF values become slowly and stably decreasing or increasing as the h/a is greater than 1.0. As shown in Table 9, the maximum values of the mode III SIF are 0.00118 and 0.00584 for $h/a = 0.1$ and $h/a = 4.0$, respectively. Hence, the values of the mode III SIF do not increase significantly as h/a increases.

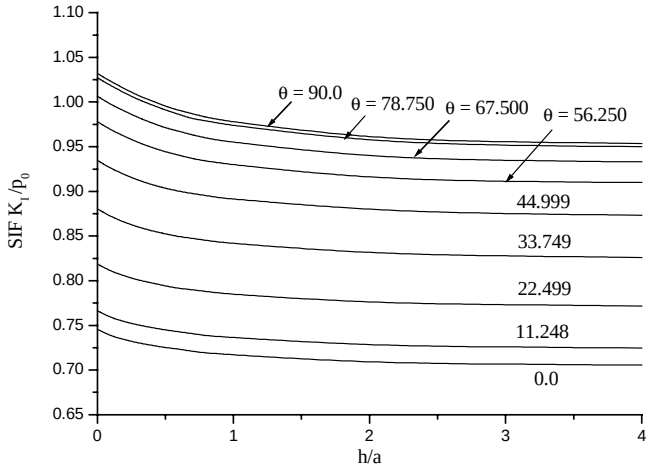

Fig. 13. Variation of Mode I SIF values for an elliptical crack in the FGM with h/a for different θ values at $a = 1.0$, $v = 0.3$, and $\alpha = 0.5$.

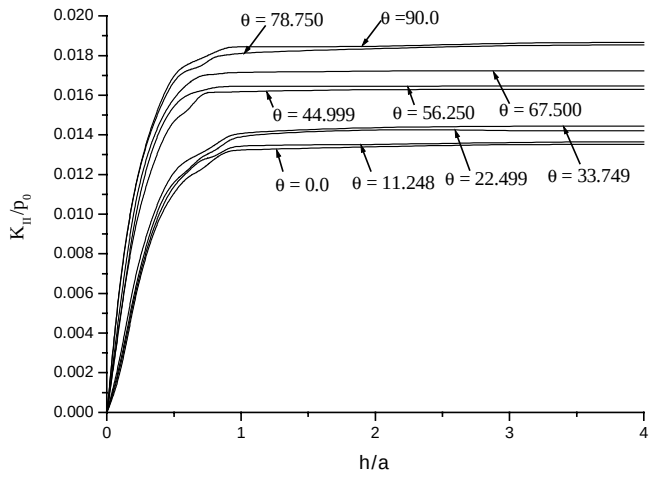

Fig. 14. Variation of Mode II SIF values for an elliptical crack in the FGM with h/a for different θ values at $a = 1.0$, $v = 0.3$, and $\alpha = 0.5$.

Table 7
Variation of the SIF value (K_I/p_0) with h/a and θ at $a = 1.0$ and $\alpha = 0.5$

h	θ								
	0.000	11.248	22.499	33.749	44.999	56.250	67.500	78.750	90.000
0.0	0.74580	0.76659	0.81884	0.88039	0.93468	0.97784	1.00651	1.02729	1. 03206
0.1	0.73818	0.75872	0.81045	0.87164	0.92575	0.96868	0.99721	1.01817	1. 02301
0.2	0.73399	0.75420	0.80523	0.86532	0.91861	0.96149	0.98993	1.01003	1. 01474
0.3	0.73049	0.75053	0.80079	0.86014	0.91269	0.95480	0.98272	1.00268	1. 00713
0.4	0.72780	0.74763	0.79750	0.85601	0.90767	0.94931	0.97668	0.99694	1. 00131
0.5	0.72512	0.74481	0.79432	0.85252	0.90336	0.94408	0.97118	0.99107	0. 99547
0.6	0.72349	0.74276	0.79142	0.84941	0.90030	0.94061	0.96703	0.98609	0. 99049
0.7	0.72089	0.74074	0.78994	0.84746	0.89757	0.93667	0.96307	0.98123	0. 98700
0.8	0.71903	0.73870	0.78796	0.84514	0.89534	0.93383	0.95976	0.97900	0. 98292
0.9	0.71838	0.73755	0.78616	0.84321	0.89280	0.93207	0.95724	0.97609	0. 98035
1.0	0.71691	0.73649	0.78461	0.84173	0.89141	0.92981	0.95489	0.97362	0. 97774
2.0	0.70804	0.72729	0.77501	0.83033	0.87865	0.91418	0.93786	0.95551	0. 95903
3.0	0.70661	0.72595	0.77314	0.82772	0.87490	0.91093	0.93436	0.95139	0. 95535
4.0	0.70569	0.72449	0.77175	0.82619	0.87322	0.90984	0.93306	0.94988	0. 95374

Table 8
Variation of the SIF value (K_{II}/p_0) with h/a and θ at $a = 1.0$ and $\alpha = 0.5$

h	θ								
	0.000	11.248	22.499	33.749	44.999	56.250	67.500	78.750	90.000
0.0	−0.00551	−0.00586	−0.00641	−0.00576	−0.00372	−0.00208	−0.00255	−0.00414	−0.00497
0.1	0.00175	0.00205	0.00230	0.00263	0.00490	0.00468	0.00548	0.00695	0.00701
0.2	0.00556	0.00580	0.00602	0.00667	0.00918	0.00967	0.01042	0.01120	0.01120
0.3	0.00815	0.00835	0.00862	0.00909	0.01163	0.01254	0.01304	0.01370	0.01380
0.4	0.00998	0.01025	0.01063	0.01095	0.01354	0.01440	0.01478	0.01544	0.01569
0.5	0.01111	0.01149	0.01169	0.01222	0.01485	0.01552	0.01590	0.01682	0.01713
0.6	0.01191	0.01210	0.01216	0.01275	0.01513	0.01606	0.01659	0.01731	0.01758
0.7	0.01219	0.01279	0.01292	0.01306	0.01613	0.01622	0.01703	0.01740	0.01785
0.8	0.01280	0.01285	0.01315	0.01345	0.01616	0.01640	0.01704	0.01800	0.01815
0.9	0.01321	0.01334	0.01370	0.01394	0.01615	0.01645	0.01714	0.01801	0.01844
1.0	0.01325	0.01348	0.01403	0.01414	0.01619	0.01645	0.01715	0.01816	0.01844
2.0	0.01340	0.01350	0.01430	0.01440	0.01630	0.01645	0.01722	0.01835	0.01843
3.0	0.01352	0.01363	0.01420	0.01444	0.01630	0.01646	0.01723	0.01852	0.01865
4.0	0.01352	0.01365	0.01420	0.01444	0.01630	0.01646	0.01724	0.01854	0.01866

5. Summary and conclusions

A novel GKS-BEM has been used for accurate and efficient evaluations of the crack problems in FGM material systems. The GKS-BEM is based on the GKSs in multi-layered elastic solids. Traction-singular elements were used to capture the singularities at the crack tip in the FGM and the multi-region method of the conventional BEM was adopted to treat the two co-planar crack surfaces. The layered discretization technique was used to approximate the FGM as a large number of dissimilar sub-layers.

The paper presented the calculation results of the SIF values for a penny-shaped or an elliptical crack in the two bonded materials through a FGM layer. The accuracy and efficiency of the GKS-BEM method

Table 9
Variation of the SIF value (K_{III}/p_0) with h/a and θ at $a = 1.0$ and $\alpha = 0.5$

h	θ						
	78.750	11.248	67.500	22.499	33.749	56.250	44.999
0.0	−0.00025	0.00061	−0.00020	0.00084	0.00056	−0.00005	0.00024
0.1	0.00013	0.00039	0.00062	0.00094	0.00079	0.00118	0.00102
0.2	0.00069	0.00101	0.00138	0.00181	0.00204	0.00207	0.00227
0.3	0.00115	0.00133	0.00213	0.00236	0.00296	0.00286	0.00322
0.4	0.00139	0.00154	0.00264	0.00275	0.00362	0.00359	0.00395
0.5	0.00162	0.00169	0.00301	0.00314	0.00403	0.00397	0.00453
0.6	0.00176	0.00186	0.00324	0.00332	0.00434	0.0043	0.00476
0.7	0.00189	0.00212	0.00337	0.00342	0.00461	0.00460	0.00502
0.8	0.00214	0.00224	0.00364	0.00366	0.00482	0.00479	0.00518
0.9	0.00227	0.00231	0.00366	0.00379	0.00505	0.00481	0.00536
1.0	0.00228	0.00232	0.00377	0.00388	0.00506	0.00493	0.00552
2.0	0.00232	0.00239	0.00411	0.00425	0.00551	0.00524	0.00573
3.0	0.00236	0.00244	0.00411	0.00422	0.00562	0.00532	0.00576
4.0	0.00238	0.00244	0.00412	0.00421	0.00562	0.00539	0.00584

have been demonstrated. The SIF values are in very good agreement with the results available in the relevant literature. In this study, we have successfully approximated the FGM layer as a fully bonded sublayer system with the $n = 90$ in analyzing the influence of the FGM thickness on the SIF values. The corresponding computational time in a personal computer was limited. It is believed that the high accuracy of the SIF values can be obtained for any crack problems in the FGM material systems.

The paper further showed that the different Poisson's ratio of the FGM system do not have significant effects on the SIF values. The paper further examined the influence of material non-homogeneity parameters α and the thickness ratio h/a on the SIF of the elliptical crack. We consider that the present GKS-BEM method can be further applied to various crack problems involving the FGM materials.

Acknowledgements

The authors would like to thank the financial supports from the Research Grants Council of Hong Kong SAR Government and the Committee on research and Conference Grants of The University of Hong Kong. The authors would also like to thank the two peer reviewers and the Editor-in-Chief Professor Charles R. Steele for their valuable comments and suggestions which have greatly improved the manuscript presentation.

References

Aliabadi, M.H., 1997. Boundary element formulations in fracture mechanics. Appl. Mech. Rev. 50, 83–96.

Atkinson, C., List, R.D., 1978. Steady state crack propagation into media with spatially varying elastic properties. Int. J. Engng. Sci. 16, 717–730.

Chen, Y.F., Erdogan, F., 1996. The interface crack problem for a nonhomogeneous coating bonded to a homogeneous substrate. J. Mech. Phys. Solids 44, 771–787.

Delale, F., Erdogan, F., 1983. The crack problem for a nonhomogeneous medium. ASME J. Appl. Mech. 50, 609–614.

Delale, F., Erdogan, F., 1988. On the mechanical modeling of the interfacial regions in bonded materials. ASME J. Appl. Mech. 55, 317–324.

Dhaliwal, R.S., Singh, B.M., 1978. On the theory of elasticity of a non-homogeneous medium. J. Elasticity 8, 211–219.
Erdogan, F., 2000. Fracture mechanics. Int. J. Solids Struct. 37, 171–183.
Erdogan, F., Ozturk, M., 1992. Diffusion problems in bonded nonhomogeneous materials. Int. J. Engng. Sci. 30, 1507–1523.
Erdogan, F., Kaya, A.C., Joseph, P.F., 1991a. The crack problem in bonded nonhomogeneous materials. ASME J. Appl. Mech. 58, 410–418.
Erdogan, F., Kaya, A.C., Joseph, P.F., 1991b. The mode III crack problem in bonded materials with a nonhomogeneous interfacial zone. ASME J. Appl. Mech. 58, 419–427.
Gu, P., Asaro, R.J., 1997. Cracks in functionally graded materials. Int. J. Solids Struct. 34, 1–17.
Gu, P., Dao, M., Asaro, R.J., 1999. A simplified method for calculating the crack-tip field of functionally graded materials using the domain integral. ASME J. Appl. Mech. 66, 101–108.
Jia, Z.H., Shippy, D.J., Rizzo, F.J., 1989. Three-dimensional crack analysis using singular boundary elements. Int. J. Numer. Meth. Engng. 28, 2257–2273.
Jin, Z.H., Batra, Z.H., 1996. Some basic fracture mechanics concepts in functionally graded materials. J. Mech. Phys. Solids 44, 1221–1235.
Jin, Z., Noda, N., 1994. Crack-tip singular fields in nonhomogeneous materials. J. Appl. Mech. 61, 738–740.
Kim, J.H., Paulino, G.H., 2002. Finite element evaluation of mixed mode stress intensity factors in functionally graded materials. Int. J. Numer. Meth. Engng. 53, 1903–1935.
Lachat, J.C., Waston, J.O., 1976. Effective treatment of boundary integral equations: A formulation for three-dimensional elastostatics. Int. J. Numer. Meth. Engng. 10, 991–1005.
Luchi, M.L., Rizzuti, S., 1987. Boundary elements of for three-dimensional elastic crack analysis. Int. J. Numer. Meth. Engng. 24, 2253–2271.
Noda, N., Jin, Z., 1993. Thermal stress intensity factors for a crack in a strip of a functionally gradient material. Int. J. Solids Struct. 30, 1039–1056.
Noda, N., Wang, B.L., 2002. The collinear cracks in an inhomogeneous medium subjected to transient load. Acta Mech. 153, 1–13.
Ozturk, M., Erdogan, F., 1995. An axisymmetric crack in bonded materials with a nonhomogeneous interfacial zone under torsion. ASME J. Appl. Mech. 55, 116–125.
Ozturk, M., Erdogan, F., 1996. Axisymmetric crack problem in bonded materials with a graded interfacial region. Int. J. Solids Struct. 33, 193–219.
Pan, E., Amadei, B., 1999. Boundary element analysis of fracture mechanics in anisotropic bimaterials. Engng. Anal. Bound. Elem. 23, 681–691.
Tada, H., Paris, C., Irwin, G.R., 2000. The Stress Analysis of Cracks Handbook, third ed. ASME Press/Professional Engineering Publishing, New York/London.
Wang, B.L., Han, J.C., Du, S.Y., 2000. Cracks problem for non-homogeneous composite material subjected to dynamic loading. Int. J. Solids Struct. 37, 1251–1274.
Yue, Z.Q., 1995. On generalized Kelvin solutions in a multi-layered elastic medium. J. Elasticity 40, 1–43.
Yue, Z.Q., Xiao, H.T., 2002. Generalized Kelvin solution based boundary element method for crack problems in multi-layered solids. Engng. Anal. Bound. Elem. 26, 691–705.
Yue, Z.Q., Yin, J.H., Zhang, S.Y., 1999. Computation of point load solutions for geo-materials exhibiting elastic non-homogeneity with depth. Comput. Geotech. 25, 75–105.
Yuuki, R., Cho, S.B., 1989. Efficient boundary element analysis of stress intensity factors for interface cracks in dissimilar materials. Engng. Fract. Mech. 34, 179–188.